

Simplified equations of the compliant matrix for right elliptical flexure hinges

Jinjiang Fu, Changxiang Yan, Wei Liu, and Ting Yuan

Citation: *Review of Scientific Instruments* **86**, 115115 (2015); doi: 10.1063/1.4936212

View online: <http://dx.doi.org/10.1063/1.4936212>

View Table of Contents: <http://scitation.aip.org/content/aip/journal/rsi/86/11?ver=pdfcov>

Published by the [AIP Publishing](#)

Articles you may be interested in

[Design and analysis of a high-accuracy flexure hinge](#)

Rev. Sci. Instrum. **87**, 055106 (2016); 10.1063/1.4948924

[Fuzzy multi-objective optimization for movement performance of deep-notch elliptical flexure hinges](#)

Rev. Sci. Instrum. **86**, 065005 (2015); 10.1063/1.4922914

[Damped leaf flexure hinge](#)

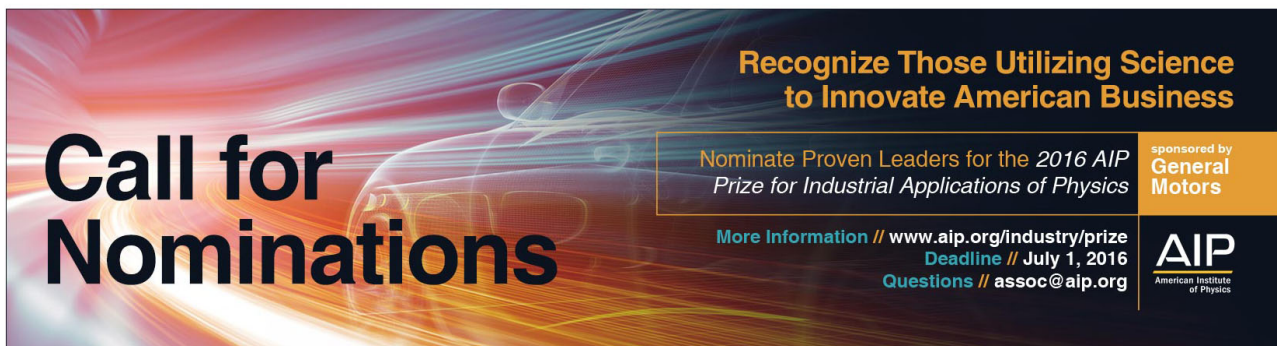
Rev. Sci. Instrum. **86**, 055002 (2015); 10.1063/1.4920992

[Hybrid flexure hinges](#)

Rev. Sci. Instrum. **84**, 085004 (2013); 10.1063/1.4818522

[Elliptical flexure hinges](#)

Rev. Sci. Instrum. **68**, 1474 (1997); 10.1063/1.1147635



Call for Nominations

Recognize Those Utilizing Science to Innovate American Business

Nominate Proven Leaders for the *2016 AIP Prize for Industrial Applications of Physics*

More Information // www.aip.org/industry/prize
Deadline // July 1, 2016
Questions // assoc@aip.org

sponsored by
General Motors

AIP
American Institute of Physics

Simplified equations of the compliant matrix for right elliptical flexure hinges

Jinjiang Fu,^{1,2} Changxiang Yan,¹ Wei Liu,¹ and Ting Yuan^{1,2}

¹Changchun Institute of Optics, Fine Mechanics and Physics, Chinese Academy of Science, 130033 Changchun, China

²University of Chinese Academy of Sciences, 100049 Beijing, China

(Received 27 March 2015; accepted 9 November 2015; published online 24 November 2015)

The simplified compliance matrix for right elliptical hinges is presented in this paper by nonlinear curve fitting on the basis of the equations derived by Chen *et al.* [Rev. Sci. Instrum. **79**, 095103 (2008)]. The equations of the rotation stiffness are then confirmed by comparison with results from finite element analysis and experimental measurements. Percentage errors between theoretical predictions and results from both the finite element analysis and experimental testing are within 5% for a range of geometries with the ratio s (b/t) between 1 and 14. The geometric parameter optimization for the purposes of maximizing the rotation stiffness for one universal hinge is utilized to illustrate the application of the simplified equations. The theoretical predictions are in good agreement with both the result of simulation and experiment for the universal hinge: the error between them is within 6.5%. © 2015 AIP Publishing LLC. [<http://dx.doi.org/10.1063/1.4936212>]

I. INTRODUCTION

In planar-compliant mechanisms, flexure hinges are beam-like cutout portions, which deform under loading by the elastic characteristic of the matter and it can allow motion transmission between the rigid members attached by the flexure hinges. In general, the flexure hinges play the role of revolute pairs as the function of bearings. Comparing to the conventional joints, it has several advantages, such as: zero friction and backlash, high resolution, compact, no need of assembly, easy to fabricate by the available high-precision production technologies such as precision milling, electro-discharge machining (EDM), lithography-based micro-manufacturing technologies, etc, and the resulting monolithic devices reaction to unforeseen external impact. Compliant mechanisms with flexure hinges are widely used in robotics, high-accuracy alignment devices for optical fibers, piezo-flexural positioning stages, and nanopositioning stages where high precision¹⁻⁴ is required in a relatively small range.

The single-axis flexure hinge may be divided into two broad categories: leaf hinges and notch hinges. The notch hinges can be altered through their geometric configuration by using various curves to define the in-plane thickness of the hinges. So notch hinges can be divided into different kinds: circular hinges, elliptical hinges, parabolic hinges, hyperbolic hinges, Bézier curve hinges, hybrid hinges, etc.

As the critical parts of compliant mechanisms, flexure hinges have been designed and researched in previous works. In 1965, the circular flexure hinges were introduced by Paros and Weisbord⁵ who presented both the exact and simplified design equations for calculating the compliances of the circular flexure hinges according to Euler-bernoulli beam model. In 2002, Wu and Zhou⁶ deduced more concise and exact equations than those of Paros and Weisbord for the

circular flexure hinges. In 2001, Lobontiu *et al.*⁷ studied right circularly corner-filletted flexure hinges, while compliance of parabolic and hyperbolic hinges is given in 2002.⁸ In 2010, Tian *et al.*⁹ presented dimensionless empirical equations and graph expressions of filletted V-shaped flexure hinges. As for hybrid flexure hinges: In 2013, Lobontiu *et al.*¹⁰ researched the right circularly corner-filletted parabolic flexure hinge and in 2014, Lin *et al.*¹¹ introduced a hybrid flexure hinge composed of half a hyperbolic flexure hinge and half a corner-filletted flexure hinge. The hybrid flexure hinges are then compared with five kinds of common notch flexure hinges (circular, corner-filletted, elliptical, hyperbolic, and parabolic flexure hinges) quantitatively based on compliance, precision, compliance precision ratios, and the maximum stress.

Right elliptical hinges, which are intermediate between circular hinge and leaf type hinge, were first proposed and studied by Smith *et al.*¹² who presented closed-form equations for the elliptical flexure hinges based on modification of the work of Paros and Weisbord in 1997. The accuracy of the closed form equations are assessed and verified by finite element analysis (FEA) and experimentation. In 2008, Chen *et al.*¹³ proposed elliptical arc flexure hinges, which brings circular right-circular and elliptical profiles together and deduced the compliance matrix by introducing the eccentric angle of ellipse as the integral variable. In 2011, Chen *et al.*¹⁴ calculated the stiffness analytically and numerically of the elliptical-arc-filletted flexure hinges.

The research mentioned above is mostly concentrated on the calculation of the compliance matrix for different kinds of flexure hinges. Another main topic about the flexure hinges is the optimization of the flexure hinges. Chen *et al.*¹⁵ presented geometrical profile optimization of elliptical flexure hinge using the modified particle swarm algorithm in 2005. Hwang *et al.*¹⁶ finished optimal design of a flexure-hinge precision stage with a lever in 2007. In 2009, Zelenika *et al.*¹⁷ proposed

an integrated approach to the optimized design of flexural hinges based on a parametric finite element model, allowing freeform optimized hinge shape to be obtained.

From the above analysis, we can conclude that the equations to calculate the stiffness for elliptical hinges are accurate. Considering the speed and efficiency of the optimization or the structural design without complex computing tools, however, they are not concise enough. In this paper, we propose simplified and accurate equations to calculate the compliant matrix of the right elliptical hinges by means of nonlinear curve fitting with Matlab software. By using the simplified equations, we present the parameters optimization of the elliptical hinge to maximize the rotation stiffness analytically.

II. NONLINEAR CURVE FITTING

For right elliptical hinge of Fig. 1 ($\phi_m = \pi/2$), one end is fixed, while the other end is free. By defining the force and moment on the hinge by $F = [F_x, F_y, F_z, M_x, M_y, M_z]$ and the corresponding deformations of the hinge by $D = [\delta_x, \delta_y, \delta_z, \theta_x, \theta_y, \theta_z]$, so the following relationship can be ob-

tained:

$$D = C_h F, \tag{1}$$

where C_h is the compliance matrix of the hinge, which can be expressed by

$$C_h = \begin{pmatrix} \frac{\delta_x}{F_x} & 0 & 0 & 0 & 0 & 0 \\ 0 & \frac{\delta_y}{F_y} & 0 & 0 & 0 & \frac{\delta_y}{M_z} \\ 0 & 0 & \frac{\delta_z}{F_z} & 0 & \frac{\delta_z}{M_y} & 0 \\ 0 & 0 & 0 & \frac{\theta_x}{M_x} & 0 & 0 \\ 0 & 0 & \frac{\theta_y}{F_z} & 0 & \frac{\theta_y}{M_y} & 0 \\ 0 & \frac{\theta_z}{F_y} & 0 & 0 & 0 & \frac{\theta_z}{M_z} \end{pmatrix}. \tag{2}$$

The approximate compliance matrix was presented by Chen *et al.*¹³ and the most important element of the matrix is the angular compliance around the flexure axis Z given by

$$\frac{1}{K_{\theta_z, M_z}} = \frac{12a}{Ewt^3} \frac{(12s^2 + 8s + 2) \sqrt{4s + 1} + 12s(2s + 1)^2 \arctan \sqrt{4s + 1}}{(4s + 1)^{5/2} (2s + 1)},$$

$$\text{Assume } N2 = f(s) = \frac{(12s^2 + 8s + 2) \sqrt{4s + 1} + 12s(2s + 1)^2 \arctan \sqrt{4s + 1}}{(4s + 1)^{5/2} (2s + 1)} \tag{3}$$

$$\Rightarrow \frac{1}{K_{\theta_z, M_z}} = \frac{12af(s)}{Ewt^3},$$

where $f(s)$ is a dimensionless stiffness factor, a is the half length of the major axis, b is the half length of the minor axis, t is the minimum thickness of the flexure hinge, w is the depth of the hinges, E is the elastic modulus, s is the dimensionless factor and $s = b/t$.

Eq. (3) is accurate for rotation stiffness calculation but not concise. In order to obtain the simplified equation, we simplify the dimensionless compliance factor $f(s)$ by nonlinear curve fitting. The function $f(s)$ was fitted by different models (power function, exponential, a second-degree polynomial, and a

third-degree polynomial). The results of the fittings are shown in Fig. 2. Residuals analysis showed that power function fitting is better than the other three kinds of fittings and the maximum residuals are less than 0.05.

The fitting function got by power function fitting is given by

$$f'(s) = ms^n = 1.122s^{-0.485}. \tag{4}$$

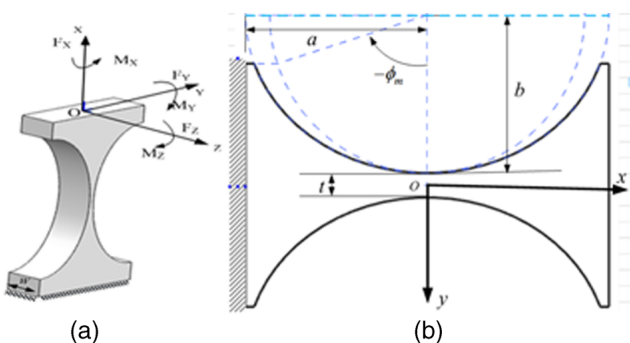


FIG. 1. (a) Model and (b) profile of elliptical flexure hinge.

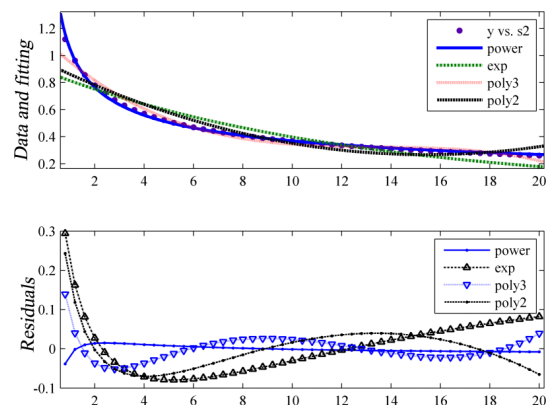


FIG. 2. The figure of the fitting curve and residuals.

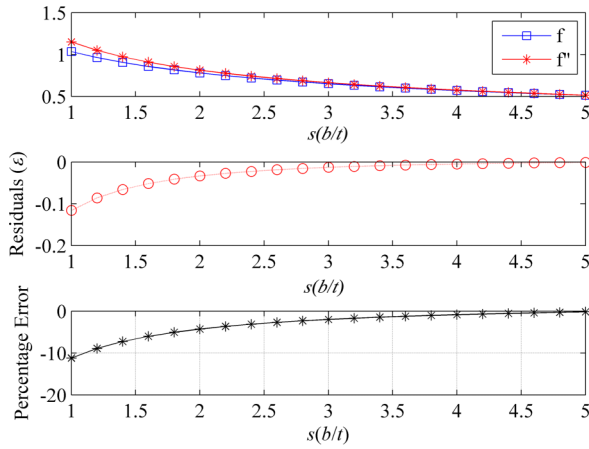


FIG. 3. Comparison between functions $f(s)$ and f'' .

This function is not concise enough, so we replace the coefficients m, n with $1.15, -0.5$, so,

$$f''(s) = as^b = 1.15s^{-1/2}. \quad (5)$$

The curves of the function $f(s), f''(s)$, residuals, and percentage error between $f(s)$ and $f''(s)$ are plotted in Fig. 3. The percentage error is larger than 4.2% when the variable s is less than 2 and the percentage error is within 2.0%, while the variable s is greater than 3.

In order to reduce percentage error when s is between 0 and 2, we re-fit the function $f(s)$ using a power function with constant term. The result is shown in Fig. 4. The new fitting function is given by

$$f'''(s) = Ms^N + p = -1.2s^{0.35} + 2.27. \quad (6)$$

The simplified expression for the rotation stiffness can be obtained by substituting Eqs. (5) and (6) into Eq. (3), respectively, yields

$$K'_{\theta_z, M_z} = \begin{cases} \frac{Ewt^3}{12a(-1.2s^{0.35} + 2.27)}, & 0 < s \leq 2, \\ \frac{Ewt^{\frac{5}{2}}b^{\frac{1}{2}}}{13.8a}, & s > 2. \end{cases} \quad (7)$$

The seminal work on the elliptical flexure hinges was done by Smith and co-workers¹² in 1997. The full-fledged rotation

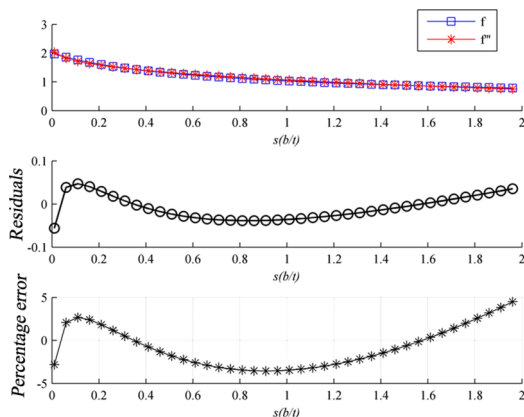


FIG. 4. Comparison between functions $f(s)$ and $f'''(s)$.

stiffness equation around the elliptical flexure axis is given by

$$K_{\theta_z, M_z - Smith} = \frac{2Eba_x^2}{3\epsilon^3 f(\epsilon\beta_x)}, \quad (8)$$

where $f(\beta) = \left(\frac{1}{2\beta + \beta^2}\right) \left\{ \frac{3 + 4\beta + 2\beta^2}{(1 + \beta)(2\beta + \beta^2)} + \frac{6(1 + \beta)}{(2\beta + \beta^2)^{3/2}} \tan^{-1}\left(\sqrt{\frac{2 + \beta}{\beta}}\right) \right\}$. The relative errors between Eqs. (7) and (8) will be discussed in Section IV.

The other simplified equations of the compliance matrix shown in Eq. (2) are listed below. In these equations, except for bending produced by forces and moments, axial loading, shearing, and torsional effect are taken into account,

$$\frac{\delta X}{F_X} = \frac{\theta_Y}{M_Y} / \left(\frac{12}{w^2}\right) = \frac{\delta Z}{M_Y} / \left(-\frac{12a}{w^2}\right) = \frac{\theta_Y}{F_Z} / \left(-\frac{12a}{w^2}\right) = \frac{a}{Ewt} H1, \quad (9)$$

$$\frac{\delta Y}{F_Y} = \frac{24a^3}{Ewt^3} H2 - \frac{12a^3}{Ewt^3} H4 + \frac{Ka}{Gwb} H1, \quad (10)$$

$$\frac{\delta Z}{F_Z} = \left(\frac{24a^3}{Ew^3t} + \frac{Ka}{Gwb}\right) H1 - \frac{12a^3}{Ew^3t} H3, \quad (11)$$

$$\frac{\theta_X}{M_X} = \frac{7a}{2Gw^3t} H1 + \frac{7a}{2Gwt^3} H2, \quad (12)$$

$$H1 = \frac{24}{5} s^{-\frac{3}{40}} - 3.25, \quad (13)$$

$$H2 = \begin{cases} 1.15s^{-1/2} & s > 2 \\ -1.2s^{0.35} + 2.27 & s \leq 2 \end{cases}, \quad (14)$$

$$H3 = -2.48s^{\frac{3}{40}} + 3.6, \quad (15)$$

$$H4 = 1.24s^{-0.24} - 0.35. \quad (16)$$

The percentage errors between the simplified functions $H2$ and the exact functions $N2$ are shown in Figs. 3 and 4. The percentage errors between the simplified functions ($H1, H3, H4$) and the exact functions ($N1, N3, N4$) are plotted in Fig. 5, respectively. The errors between the simplified equations of $H1, H2, H3$, and $H4$ proposed in this paper and the exact equations of $N1, N2, N3$, and $N4$ presented by Chen *et al.*¹³ are less than 4% when the variable s is between 1 and 15, respectively.

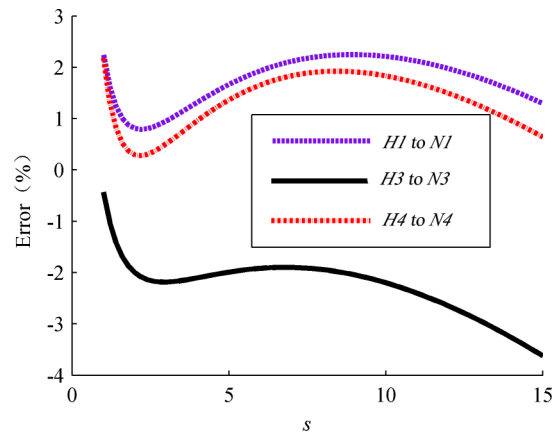


FIG. 5. Percentage error between the exact functions ($N1, N3, N4$) and the simplified functions ($H1, H3, H4$).

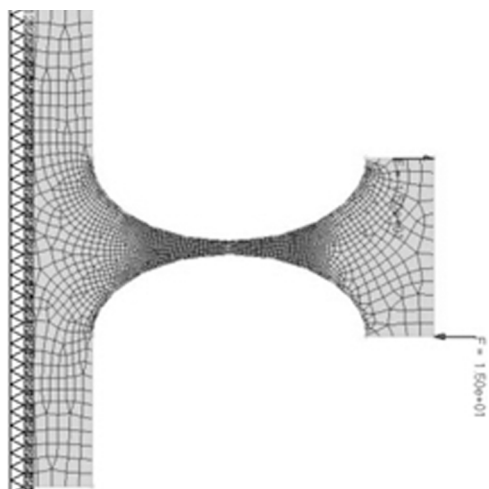


FIG. 6. The finite element model for the right elliptical hinge.

III. VERIFICATION OF THE SIMPLIFIED EQUATIONS

Both finite element analysis and experimental testing have been used to assess the accuracy of simplified Eq. (7). Before the finite element simulation, we need to know the accuracy of stiffness estimates for a notch type hinge.

A. Finite element analysis

Models for the finite element analysis were generated with the Altair Hyperworks package. In an effort to assess the validity of Eq. (7), a variety of right elliptical hinge configurations were assessed. One finite element model is shown in Fig. 6. The model uses thin shell elements, which owes six degrees of freedom and consists of 2376 elements. The left end of the model was fixed and the bending moment is applied in the right end. The global element size is 1 mm and the local element size within the notch region is 0.15 mm.

The numerical accuracy of the finite element simulation is relative to the size, type, and distribution of the elements. To determine the necessary element size for an acceptable accuracy, a number of models with the same geometric shape were studied with different element sizes. The results of the analysis and the input parameters of the model are summarized in Table I. It was not until the local element size was reduced to one fifth of the thickness t that the result errors of the finite element analysis were less than 1%, which is within the analytical model's error band.

TABLE I. Values of right elliptical hinge stiffness and precision as a function of element size.

M (N · m)	a (mm)	b (mm)	t (mm)	w (mm)	E (GPa)
$15 \cdot 13 \cdot 0.001$	10	6	1	8	106
Local element size (mm)	Number of elements			θ (mrad)	Stiffness (N · m/rad)
1	288			10.90	17.89
0.8	360			10.19	19.14
0.6	448			12.78	15.26
0.4	737			12.95	15.06
0.2	1596			13.05	14.94
0.15	2376			13.07	14.92
0.1	5089			13.07	14.92

Using meshes of the local element size less than one fifth of the thickness t , the stiffness values were analyzed for a variety of right elliptical hinges. The minimum thickness t of the model is 1 mm, so the global element size 1 mm and the local element size 0.15 mm are adopted to finish the finite element analysis. The results from finite element analysis and theoretical predictions given by Eqs. (7) and (8) are shown in Table II. The percentage errors between them are shown in Fig. 7. It reveals that all of the percentage errors are less than 5%.

B. Experiment testing

An experiment was performed to determine the rotation stiffness for a range of right elliptical hinges to verify the validity of simplified Eq. (7). Five flexure hinge samples are machined by the wire cut electrical discharge machine on an 8 mm thick titanium alloy stock (Tc4). The Young's modulus of the material is theoretically estimated to be $E = 106$ GPa. The other geometric parameters are listed in Table I.

The schematic and the setup of the experimental testing are shown in Fig. 8. The setup comprises a photoelectric auto-collimator (0.2 in. resolution), hinge samples, base plate, connecting plate, small size mirror attached to the connecting plate, known masses, and thin wire.

Rotation stiffness is evaluated by placing known masses on the connecting plate with a fine thin wire and noting the subsequent rotation angle measured by photoelectric auto-collimator. The experimental rotation stiffness can be obtained

$$K_{exp} = M/\theta = mgL \cos \theta/\theta, \tag{17}$$

TABLE II. Results from finite element analysis and the theoretical calculation.

No. of elements	S (b/t)	a (mm)	b (mm)	M (N · mm)	Θ (mrad)	K-fem (N m/rad) (FEM)	K-smith (N m/rad) (Eq. (8))	K-app (N · m/rad) (Eq. (7))
1424	1	10	1	150	22.12	6.78	6.83	6.6
1578	2	10	2	250	26.96	9.27	9.06	9.54
1874	4	10	4	450	36.03	12.49	12.40	12.29
2376	6	10	6	650	43.56	14.92	15.01	15.05
2512	8	10	8	850	49.26	17.26	17.24	17.38
3084	10	10	10	1050	55.69	18.85	19.21	19.43
6436	12	20	12	1250	114.47	10.92	10.50	10.64
6801	14	20	14	1450	122.31	11.86	11.32	11.5

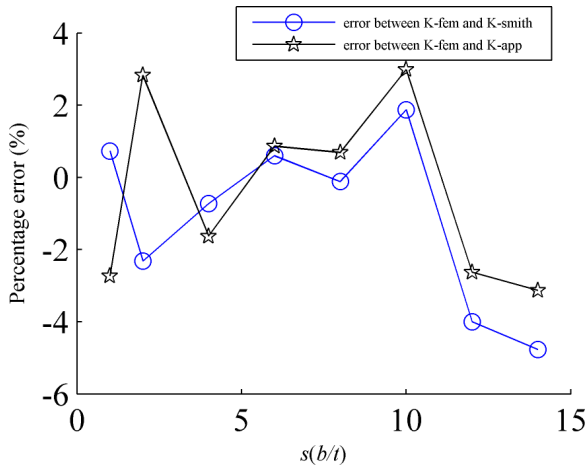


FIG. 7. Percentage error between finite element analysis and theoretical predictions (by Eqs. (7) and (8)) for right elliptical hinges as a function of s .

where M is the bending moment, θ is the rotation angle, m is the mass, and L is the distance from the center of rotation to the vertical wire.

This method of testing the rotation stiffness possesses the advantages over traditional testing since the rotation angle can be noted directly. The potential error of the inclusion of measured distortion was eliminated. But, there are still a lot of potential error sources that can arise with this setup such as reading error, environmental error, manufacturing error, and so on. So as to reduce the reading error and environmental error, every test was repeated three times. The fitting curve of the flexure hinge 3 is plotted in Fig. 9 and the slope of the curve is the rotation stiffness.

Table III lists the experimental results for the five samples comparing to the theoretical simplified equation for the rotation stiffness given by Eq. (7). It is clear that the relative errors between them were less than 5%.

IV. APPLICATION

In this section, we use the simplified equations to optimize the design of the two-degree universal hinge illustrated in Fig. 10(b). The universal hinge is made of Tc4 with elastic modulus $E = 106$ GPa and it is composed of four identical right elliptical hinge shown in Fig. 10(a). It can rotate around axis X by the deflection of hinge 1 and hinge 3, while it rotates around axis Y by the deflection of hinge 2 and hinge 4. The coordinate of the single hinge is $o-xyz$ and $O-XYZ$ is the

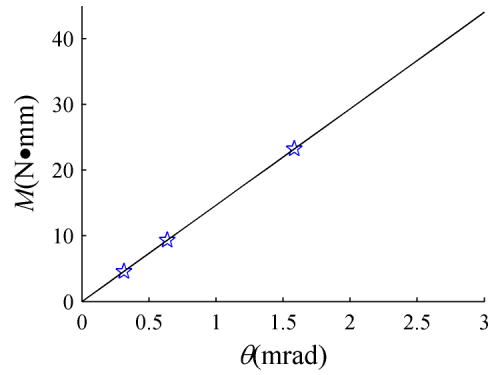


FIG. 9. Fitting curve of the flexure hinge 3.

coordinate of the universal hinge. The purpose of this design is to maximize the rotation stiffness so as to maximize the resonant frequency under the condition that the parameters E , a , b , w , σ_{max} , θ are given ($E = 106$ GPa, $a = 6$ mm, $b = 4$ mm, $w = 7.5$ mm, $\sigma_{max} = 160$ MPa, $\theta = 10$ mrad). The top of the universal hinge will connect with some mechanism and it will be actuated by piezoelectric.

According to the theory of the dynamics, the relationship between the rotation stiffness and the natural frequency for the universal hinge is given by

$$f_{umi} = \frac{1}{2\pi} \sqrt{\frac{K_X}{J_X}}, \quad (18)$$

where K_X is the rotation stiffness of the universal hinge, while J_X is the moment of inertia of the universal hinge around axis X .

A. Analytical model of the universal hinge

The rotation stiffness can be deduced by lumped parameter analysis and the model of calculating rotation stiffness (K_X , for example, K_Y can be obtained by the same way) for the universal hinge is plotted in Fig. 11. The equation of the equivalent stiffness of the universal hinge is given by Eq. (19),

$$K_X = \frac{(K_{1,\theta_z,M_z} + K_{3,\theta_z,M_z})(K_{2,\theta_y,M_y} + K_{4,\theta_y,M_y})}{(K_{1,\theta_z,M_z} + K_{3,\theta_z,M_z} + K_{2,\theta_y,M_y} + K_{4,\theta_y,M_y})}, \quad (19)$$

where K_{θ_z,M_z} represents the rotation stiffness around the axis z of the single right elliptical hinge, K_{θ_y,M_y} is the rotation stiffness around the axis y of the single right elliptical hinge. It is easy to know that $K_{1,\theta_z,M_z} = K_{3,\theta_z,M_z} = K_{\theta_z,M_z}$, $K_{2,\theta_y,M_y} = K_{4,\theta_y,M_y} = K_{\theta_y,M_y}$ and in most cases $K_{\theta_y,M_y} \gg K_{\theta_z,M_z}$.

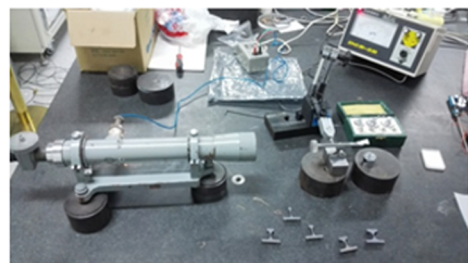
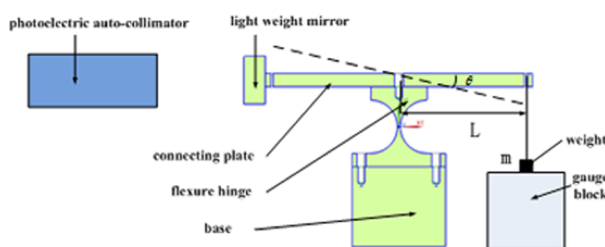


FIG. 8. (a) Schematic and (b) the setup of experimental testing for the calculation of the rotation stiffness for right elliptical hinge.

TABLE III. Experimental testing of right elliptical hinge stiffness and theoretical comparison.

Hinge No.	t_{nom} (mm)	t_{tes} (mm)	a (mm)	b (mm)	w_{nom} (mm)	w_{tes} (mm)	K_{exp}	K'_{θ_z, M_z}	Error (%)
1	1	1.010	10	2	8	8.010	9.21	9.54	3.46
2	1	1.013	10	4	8	8.015	11.70	12.29	4.82
3	1	0.985	10	6	8	7.985	14.67	15.05	2.50
4	1	1.012	10	8	8	8.006	16.71	17.38	3.84
5	1	0.992	10	10	8	7.988	19.13	19.43	1.57

Eq. (19) can be simplified to

$$K_X = \frac{2K_{\theta_z, M_z} \times 2K_{\theta_y, M_y}}{2K_{\theta_z, M_z} + 2K_{\theta_y, M_y}} \approx 2K_{\theta_z, M_z}. \quad (20)$$

According to Eqs. (18) and (20), when the moment of inertia is constant, we need to maximize the rotation stiffness of the single flexure hinge for maximizing the natural frequency. When the force F was applied in the universal hinge indicated in Fig. 10, the universal hinge will rotate around axis X . Suppose the force F is in the plane of YOZ and it is parallel with the axis Z . l is the distance between the force and the axis Z . In order to satisfy the requirements of the structural design, the distance l is equal to 12 mm. According to the theorem on translation of force, the force F can be replaced by force F' and the moment M ($F = F'$, $M = Fl$), force F' and the moment M can be translated into single flexure hinge shown in Fig. 12.

In order to express the displacement-loading relationship at the free end in xoy plane, Eq. (2) can be simplified and be written as

$$\begin{Bmatrix} \theta_z \\ y \\ x \end{Bmatrix} = \begin{bmatrix} C_{\theta_z, M_z} & C_{\theta_z, F_y} & 0 \\ C_{y, M_z} & C_{y, F_y} & 0 \\ 0 & 0 & C_{x, F_x} \end{bmatrix} \begin{Bmatrix} M_z \\ F_y \\ F_x \end{Bmatrix}. \quad (21)$$

So we can deduce that

$$\theta_z = C_{\theta_z, M_z} M_z + C_{\theta_z, F_y} F_y. \quad (22)$$

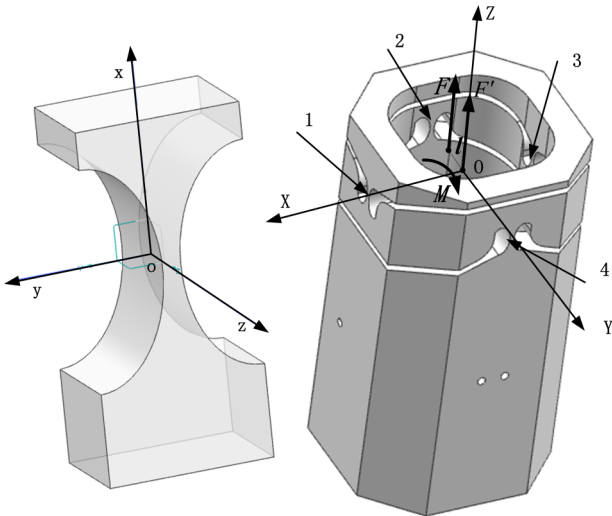


FIG. 10. Diagrams of (a) right elliptical hinge and (b) two-axis universal hinge.

When the universal hinge is at work, force $F_y = 0$, then,

$$M_z = \theta_z / C_{\theta_z, M_z} = K'_{\theta_z, M_z} \theta_z. \quad (23)$$

The maximum stress which occurs at each of the outer surfaces of the thinnest part of the elliptical hinge can be calculated from a nominal stress by equation

$$\sigma_{\max} = k_b \frac{(M_z + LF_y)}{W} + k_a \frac{F_x}{S} = \frac{k_b(M_z + LF_y)}{t^2 w / 6} + k_a \frac{F_x}{wt}, \quad (24)$$

where the stress concentration factor in bending k_b and k_a , to within better 1.7% over a wide range of elliptic flexure hinges, is given by¹⁸

$$k_b = \frac{\zeta + 0.253}{\zeta + 0.097}, \quad (25)$$

$$k_a = \frac{\zeta + 0.371}{\zeta + 0.097}, \quad (26)$$

where $\zeta = \rho/t = a^2/(bt)$, ρ is the radius of curvature of the cutouts at the notch bottom.

In this case, mechanical designs require a specific rotation angle θ ($\theta = 10$ mrad). The parameters a , b , w , E , θ for right elliptical hinge are given, substituting Eqs. (23) and (7) and $M_z = M/2$, $F_x = F'/2 = M/(2l)$, $F_y = 0$ to Eq. (24), the maximum stress is given by

$$\sigma_{\max} = \left(\frac{3k_b}{t^2 w} + \frac{k_a}{2wtl} \right) \frac{E w \theta t^{\frac{5}{2}} b^{\frac{1}{2}}}{6.9a} = \left(\frac{3k_b}{t^2} + \frac{k_a}{2tl} \right) \frac{E \theta t^{\frac{5}{2}} b^{\frac{1}{2}}}{6.9a}. \quad (27)$$

It is clear that the maximum stress is not relevant with the width w . The maximum stress increases with the increase of thickness t when the other parameters remain constant illustrated in Fig. 13. Substituting the parameters of E , a , b , w , σ_{\max} , θ to Eq. (27), we can get the maximum thickness $t = 1.019$ mm. It is evident that the rotation stiffness increases with the increase of thickness t given by Eq. (7). So when t is 1.019 mm, we can get the maximum rotation stiffness when the other parameters are given above. Considering the

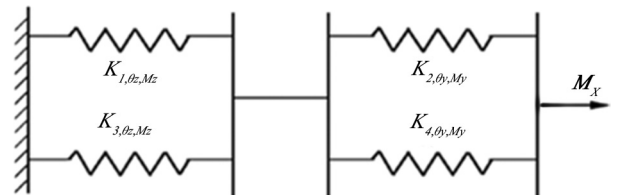


FIG. 11. Equivalent stiffness of the universal hinge.

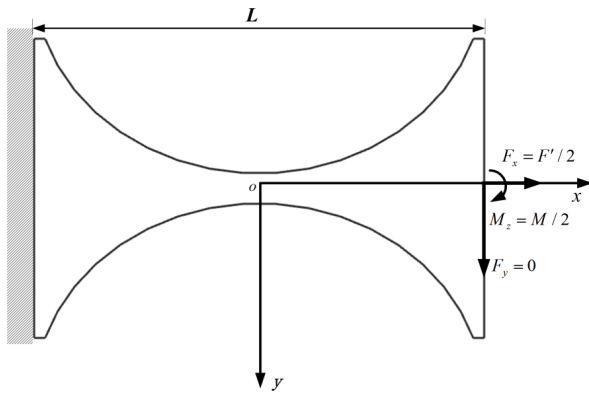


FIG. 12. Schematic representation of single flexure hinge with loading.

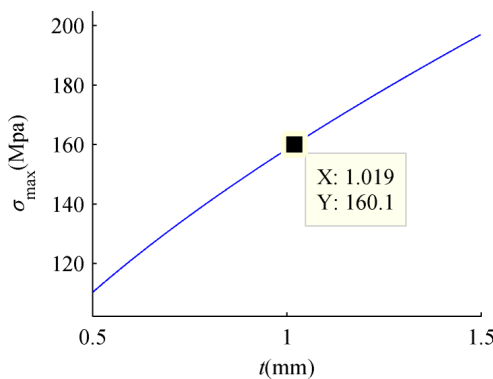


FIG. 13. The relationship between the maximum stress and the minimum thickness t ($E = 106$ GPa, $a = 6$ mm, $b = 4$ mm, $w = 7.5$ mm, $\sigma_{max} = 160$ MPa, $\theta = 10$ mrad).

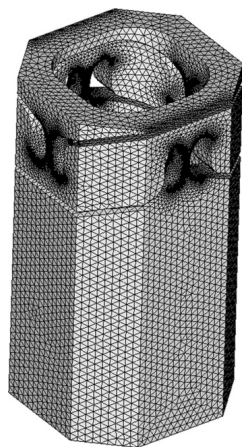


FIG. 14. Finite element model of the universal hinge.

TABLE IV. Results comparison between theoretical calculation and finite element analysis.

Force (N)	Rotation angle (mrad)	Maximum stress (MPa)	$K_{X(\text{theo})}$ (N m/rad)	$K_{X(\text{FEA})}$ (N m/rad)	Error (%)
32	9.741	143.9	38.4	39.42	-2.59
32.8	9.995	147.5			

convenience of the manufacturing and the manufacturing error, we adopted the value of $t = 1$ mm. The maximum rotation stiffness $K_{\theta_z, M_z} = 19.20$ N m/rad for the single right elliptical hinge. So the maximum rotation stiffness and the maximum stress for the universal hinge is about 38.4 N m/rad and 158.5 MPa, which is less than 160 MPa, respectively.

B. Finite element results

Fig. 14 shows the finite element model of the universal hinge. The model contains 186 757 elements and Tetra10 elements are used. The element size is 2 mm. But in order to ensure the accuracy of the finite element analysis, the minimum size of the elements in the regions of the flexure hinges is 0.2 mm. In this analysis, the universal was rigidly fixed at one end, with a bending moment M and force F' being applied to the other end of the universal hinge around axis X .

The numerical results from the finite element analysis are shown in Table IV. The theoretical stiffness for the universal hinge is relatively small than the values from finite element analysis; however, the error between them is less than 3%. The model showed in Fig. 11 is verified. When the rotation angle is 10 mrad, the maximum stress is close to but less than the value of $\sigma_{ymax} = 160$ MPa. Eq. (7) is verified to be accurate enough to maximize the rotation stiffness of the right elliptical hinge in most engineering design.

C. Experimental results

Experimentation was also used to assess the validity of the theoretical calculation of the rotation stiffness for the universal hinge. One universal hinge made of Tc4 was machined by using wire electro discharge machining technology according to the geometric parameters decided above ($a = 6$ mm, $b = 4$ mm, $w = 7.5$ mm and $t = 1$ mm). The experimental setup was shown in Fig. 15. The universal hinge was fixed to the optical platform by glue and the load mass was put on one of the top surfaces of the specimen, respectively, while the probe of the inductance micrometer contacted with the center of the other side of the top surface. The mass of the load masses is known. When the sample deformed due to the load, the inductance micrometer records the displacements of the top surface. The rotation stiffness of the sample can be evaluated by placing known load masses and the data of the inductance micrometer. The experimental result is 35.98 N m/rad. So the relative error between the results of theoretical calculation and experiment is 6.3%.

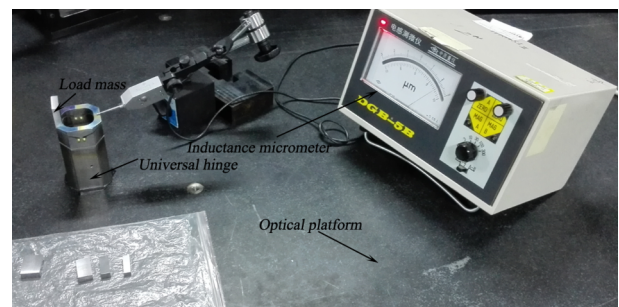


FIG. 15. The setup of the rotation stiffness testing for the universal hinge.

V. CONCLUSIONS

The simplified compliance matrix for right elliptical hinges is created by nonlinear curve fitting in this paper with an acceptable error within 5%. The equation of the rotation stiffness is verified by means of finite element analysis and experimental measurements. The simplified equation is further utilized to geometric parameter optimization of the right elliptical hinges. As an example, a universal hinge is engaged in illustrating the method of the optimal parameter design for the purposes of the maximum rotation stiffness. The results are in good agreement with both the results from the finite element analysis and the experimental testing.

- ¹T. Huang, S. Liu, J. Mei, and D. G. Chetwynd, *Mech. Mach. Theory* **70**, 246 (2013).
- ²K. Seo, S. Cho, T. Kim, H. S. Kim, and J. Kim, *Mech. Mach. Theory* **70**, 189 (2013).
- ³Y. Tian, B. Shirinzadeh, and D. Zhang, *Sens. Actuators, A* **153**, 96 (2009).
- ⁴Y. Tian, B. Shirinzadeh, and D. Zhang, *Precis. Eng.* **33**, 160 (2009).

- ⁵J. M. Paros and L. Weisbord, *Mach. Des.* **37**, 151 (1965).
- ⁶Y. Wu and Z. Zhou, *Rev. Sci. Instrum.* **73**(8), 3101 (2002).
- ⁷N. Lobontiu, J. S. N. Paine, E. Garcia, and M. Goldfarb, *J. Mech. Des.* **123**, 346 (2001).
- ⁸N. Lobontiu, J. S. N. Paine, E. O'Malley, and M. Samuelson, *Precis. Eng.* **26**, 183 (2002).
- ⁹Y. Tian, B. Shirinzadeh, and D. Zhang, *Precis. Eng.* **34**, 586 (2010).
- ¹⁰N. Lobontiu, M. Cullin, and T. Petersen, *IEEE Trans. Autom. Sci. Eng.* **11**, 169 (2014).
- ¹¹R. Lin, X. Zhang, X. Long, and S. Fatikow, *Rev. Sci. Instrum.* **84**, 085004 (2013).
- ¹²S. T. Smith, V. G. Badami, J. S. Dale, and Y. Xu, *Rev. Sci. Instrum.* **68**, 1474 (1997).
- ¹³G. Chen, X. Shao, and X. Huang, *Rev. Sci. Instrum.* **79**, 095103 (2008).
- ¹⁴G. M. Chen, X. Y. Liu, and Y. L. Du, *ASME J. Mech. Des.* **133**, 081002 (2011).
- ¹⁵G. Chen, J. Jia, and Q. Han, in *Advances in Intelligent Computing*, edited by X.-P. Z. D. S. Huang and G.-B. Huang (Springer-Verlag, Berlin, Heidelberg, 2005), p. 533.
- ¹⁶E. J. Hwang, K. S. Mine, S. H. Songd, H. Ahne, and W. C. Choia, *J. Mech. Sci. Technol.* **21**, 616 (2007).
- ¹⁷S. Zelenika, M. G. Munteanu, and F. D. Bona, *Mech. Mach. Theory* **44**, 1826 (2009).
- ¹⁸G. Chen, J. Wang, and X. Liu, *J. Mech. Des.* **136**, 031009 (2014).